Atmos. Chem. Phys. Discuss., doi:10.5194/acp-2016-458, 2016
Manuscript under review for journal Atmos. Chem. Phys.
Published: 22 June 2016

Atmospheric Chemistry and Physics Discussions

Optical and Geometrical Properties of Cirrus Clouds in Amazonia Derived From 1-year of Ground-based Lidar Measurements

Diego A. Gouveia[1], Boris Barja[1,2], Henrique M. J. Barbosa[1], Theotônio Pauliquevis[3], and Paulo Artaxo[1].

[1]Applied Physics Department. Institute of Physics, University of São Paulo (USP), São Paulo, SP, Brazil.

[2]Atmospheric Optics Group of Camagüey. Meteorological Institute of Cuba, Cuba.

[3]Department of Natural and Earth Sciences, Federal University of São Paulo, Diadema, SP, Brazil.

Correspondence to: Boris Barja Gonzalez (bbarja@gmail.com)

Abstract. For one year, from July 2011 to June 2012, a ground-based raman lidar provided atmospheric observations north of Manaus, Brazil, at an experimental site (2.89°S and 59.97°W) for long-term aerosol and cloud measurements. Upper tropospheric cirrus clouds were observed more frequently than previous reports in tropical regions. The frequency of occurrence was found to be as high as 82 % during the wet season and not lower than 55 % during the dry season. The diurnal cycle shows a minimum around local noon and maximum during late afternoon, associated with the diurnal cycle precipitation. Optical and geometrical characteristics of these cirrus clouds were derived. The mean values were 14.4 ± 2.0 km (top), 12.7 ± 2.3 km (base), 1.7 ± 1.5 km (thickness), and 0.36 ± 1.20 (cloud optical depth). Cirrus clouds were found at temperatures down to −90 °C and 7 % were above the tropopause base. The vertical distribution was not uniform and two cloud types were identified: (1) cloud base > 14 km and optical depth ~0.02, and (2) cloud base < 14 km and optical depth ~0.2. A third type, not previously reported, was identified during the wet season, between 16 and 18 km with optical depth ~0.005. The mean lidar ratio was 20.2 ± 7.0 sr, indicating a mixture of thick plates and long columns. However, the clouds above 14 km have a bimodal distribution during the dry season with a secondary peak at about 40 sr suggesting that thin plates are a major habit. A dependence of the lidar ratio with cloud temperature (altitude) was not found, thus indicating they are well mixed in the vertical. Cirrus clouds classified as subvisible (τ < 0.03) were 40 %, whilst 37.7 % were thin cirrus (0.03 < τ < 0.3) and 22.3 % opaque cirrus (τ > 0.3). Hence, not only does the central Amazon have a high frequency of cirrus clouds, but a large fraction of subvisible cirrus clouds as well. This high frequency of subvisible cirrus clouds may contaminate aerosol optical depth measured by sun-photometers and satellite sensors to an unknown extent.

1. Introduction

Cirrus clouds cover on average more than 30% of the Earth´s atmosphere, with higher fractions occurring in the Tropics, hence, are important to understanding current climate and predicting future climate (Wylie et al. 2005, Stubenrauch et al. 2006; Nazaryan et al., 2008). Several studies emphasize the important role that cirrus clouds play in the Earth's radiation budget (i.e. Liou 1986; Lynch et al. 2002; Yang et al. 2010a). Their role is twofold. Firstly, cirrus clouds may increase warming by trapping a portion of infrared radiation emitted by the Earth/atmosphere system. Secondly, cirrus clouds could cool the atmosphere by reflecting part of the incoming solar radiation back into space. The contribution of each effect and the net effect on the radiative forcing depends strongly on cirrus cloud optical properties, altitude, vertical and horizontal coverage (Liou 1986). Therefore, understanding their properties is critical to determining their effect on the albedo and greenhouse effects (Barja and Antuña, 2011, Boucher et al., 2013). Also, the tropical cirrus clouds could influence the vertical distribution of radiative heating in the tropical tropopause layer (e.g., Yang et al., 2010b; Lin et al., 2013). Noticeably, it has been shown that an accurate representation of the cirrus vertical structure in cloud radiative studies improved the results of these calculations (Khvorostyanov and Sassen, 2002; Hogan and Kew, 2005; Barja and Antuña, 2011). Recent research also shows that an increase in stratospheric water vapor are linked mainly with the occurrence of cirrus clouds in the tropical tropopause layer (TTL) (Randel and Jensen, 2013). Finally, measurements of the properties of cirrus clouds at different geographical locations are of utmost importance, potentially allowing for improvements in numerical models parameterizations and, thus, reducing the uncertainties in climatic studies.

Ground-based lidars are an indispensable tool for monitoring cirrus clouds, particularly identifying optically thin and subvisible cirrus clouds (SVC) with very low optical depth, which are undetectable by cloud radars (Comstock et al., 2002) or by passive instruments (e.g., Ackerman et al., 2008). For this reason, several studies with ground-based lidars have reported the characteristics of cirrus clouds around the globe during the last decade. There are some long-term studies reporting climatologies from midlatitude (eg. Sassen and Campbell, 2001; Goldfarb et al., 2001; Giannakaki et al., 2007; Hoareau et al., 2013) and tropical regions (eg. Comstock et al., 2002; Cadet et al., 2003; Antuña and Barja, 2006; Thorsen et al., 2011; Pandit et al., 2015). Table 1 shows an overview of these studies with different values for cirrus clouds characteristics in diverse geographical regions. There are also some short-term reports on cirrus clouds characteristics during measurement campaigns in midlatitude (e.g. Immler and Schrems, 2002a) and tropical latitudes (Immler and Schrems, 2002b, Pace et al., 2003 and references therein). Additionally, satellite-based measurements have been used to investigate the global distribution of cirrus characteristics (eg. Nazaryan et al., 2008; Sassen et al., 2009; Sassen et al., 2009; Wang and Dessler 2012, Jian et al., 2015). Characteristics of tropical and subtropical cirrus clouds have similar geometrical values and these values are higher than those in midlatitudes. The frequencies of occurrence of cirrus cloud types differ significantly between different locations.

Cirrus clouds measurements reports over tropical rain forests are scarce. Very few global studies with satellites instruments include these regions. Some studies focused on deep convection in the Amazonia reported cirrus clouds (eg. Machado et al., 2002; Hong et al., 2005, Wendisch et al., 2016), but no lidar measurements were used. Baars et al. (2012) focused on aerosol measurements with a ground-based Raman lidar, but report only one cirrus cloud case between 12 km and 16 km during September 11, 2008. Barbosa et al., (2014) describe a week of cirrus clouds measurements from 30 August to 6 September 2011 during an intensive campaign for calibration of the water vapor channel of the UV Raman lidar was

Atmos. Chem. Phys. Discuss., doi:10.5194/acp-2016-458, 2016
Manuscript under review for journal Atmos. Chem. Phys.
Published: 22 June 2016

Atmospheric Chemistry and Physics
Discussions

conducted in the ACONVEX (Aerosols, Clouds, cONVection EXperiment) site. Cirrus clouds during this period were present in 60% of the measurements. Average base and top heights were 11.5 km and 13.4 km, respectively, and average maximum backscatter occurred at 12.8 km. Most of the time, three layers of cirrus clouds were actually found.

From the above discussion, the importance of continuous and long-term observations of tropical cirrus clouds is evident. In the present study, we use one year of ground-based lidar measurements (July 2011 to June 2012) at Manaus, Brazil to investigate the seasonal and diurnal variability of geometrical (cloud top and base altitude) and optical (cloud optical depth and lidar ratio) properties of cirrus over a tropical rain forest site. In section 2, a brief description of the Raman lidar system, dataset, processing algorithms and site are given. The results and discussion are presented in section 3. We close this paper with concluding remarks in section 4.

2. Instrumentation, dataset and algorithms.

2.1. Site and instrument description

The ACONVEX (Aerosols, Clouds, cONVection EXperiment) or T0e (nomenclature of the GoAmazon2014/15 experiment sites, Martin et al. 2016) site is located up-wind from Manaus-AM, Brazil, at 2.89°S and 59.97°W, in the center of the Amazon Forest. The atmospheric observations actually began in 2011 at this site, and the objective was to operate a combination of several instruments during the upcoming years for measuring atmospheric humidity, clouds and aerosols as well as processes which lead to convective precipitation (Barbosa et al., 2014). Figure 1 gives an overview of the location where the measurements in this study was done. As with most tropical continental sites, the diurnal cycle is strong with a late afternoon peak in precipitation (Adams et al., 2013). The usual climatological seasons in Central Amazon are: the wet (December to April), dry (July and August), and the transitions wet-to-dry (May and June) and dry-to-wet (September to November) (Machado et al., 2004), however the definition may vary (e.g. Arraut et al., 2012, Tanaka et al., 2014). Deep convection is a characteristic of the region during both seasons, being more active during the wet season (Machado et al., 2002), when it is influenced by the intertropical convergence zone (ITCZ). As the ITCZ moves northward during the months of dry season, the convective activity decreases. Hence, it is to be expected that deep convection is the principal cirrus clouds formation mechanism in the region.

The lidar system (LR-102-U-400/HP, manufactured by Raymetrics Advanced Lidar Systems) operates in the UV, at 355 nm and has also two Raman channels for nitrogen (387 nm) and water vapor (408 nm). The system is tilted from the zenith 5° to avoid specular reflection of horizontally oriented ice crystals. It is automatically operated 7 days a week, only being closed between 11 am and 2 pm local time (LT is −4 UTC) to avoid the sun crossing the field of view. Detailed information about the lidar system and its characterization are given by Barbosa et al. (2014). To retrieve the particle backscatter and extinction profiles from the lidar signal, the temperature and pressure profiles were obtained from the radio soundings launched at 0 and 12 UTC from the Ponta Pelada Airport, located 28.5 km to the South (3.14°S, 59.98°W) of the experimental site.

Atmos. Chem. Phys. Discuss., doi:10.5194/acp-2016-458, 2016
Manuscript under review for journal Atmos. Chem. Phys.
Published: 22 June 2016

Atmospheric Chemistry and Physics
Discussions

2.2. Datasets

The lidar dataset used in the present study comprises measurements between July 2011 and June 2012. A total of 36,597 5-minute profiles were analyzed and only 20,752 had a signal to noise ratio (SNR) higher than 3 at the characteristic altitudes of the possible cirrus clouds occurrence (between 8 km and 20 km). Statistical tests (not shown) were conducted to obtain the lowest SNR value suitable to detect subvisible cirrus clouds, and the value 3 was selected as a threshold for obtaining a good SNR. The number of 5-min lidar profiles and number of profiles with good SNR during each month of the studied period were analyzed. July, August and September, the driest months (Figure 2) show the higher fraction of profiles with good SNR, while the wettest months have the lowest fraction of lidar profiles with good SNR (see figure S.1). The cloud fraction of low, optically thick clouds increases during this season, thereby attenuating the signal and reaching the cirrus clouds altitudes with a low SNR. The frequency was then defined as the ratio between the number of lidar profiles of 5 min with good SNR containing cirrus clouds and the total number of profiles with good SNR. This frequency does not count the number of individual clouds, but the time coverage of these clouds. Thus, the frequency of occurrence was the best estimate, for a ground-based lidar, of the fraction of time when the sky is covered with cirrus clouds of different geometric and optical characteristics.

Temperature, pressure, geopotential height, humidity and winds for the study period were obtained from the ERA Interim reanalysis (Dee et al., 2011) of European Center for Midrange Weather Forecast (ECMWF) with spatial resolution of 0.75° and temporal resolution of 6 h. This dataset was used to obtain the mean high level winds, near to the cirrus clouds habits (200 hPa). Moreover, the tropopause altitudes were obtained from vertical profiles over the site using the methodology of the World Meteorological Organization (FCM-H3-1997). A precipitation dataset for the same period was acquired from TRMM (Tropical Rainfall Measuring Mission) version 7 product 3B42 (Huffman et al., 2007) with 0.25° and 3 h of spatial and temporal resolution, respectively.

2.3. Cirrus cloud detection algorithm.

We used an automatic algorithm for the detection of cloud base, top and maximum backscattering heights, based on Barja and Aroche (2001). This algorithm assumes a monotonically decreasing intensity of the lidar signal with altitude in a clear atmosphere and searches for significant abrupt changes. These abrupt changes are marked as a possible cloud base. Examining the signal noise and the change between the possible cloud base, a true cloud base is discriminated. Then, the lowest altitude above cloud base with signal lower than that at cloud base and corresponding to a molecular gaseous atmosphere is determined as the cloud top. When more than one cloud is present in the same profile, and their top and base are separated more than 400 m, they are considered as individual clouds. Figure S.2 gives an example of the cloud detection algorithm. Barbosa et al. (2014) provide details on the fully automated algorithm, which includes discrimination of false alarm and distinguishing aerosols from thin cloud layers. After obtaining the base, top and maximum backscatter heights, the corresponding cloud temperatures is obtained from the nearest radiosonde. A detected high cloud is classified as a cirrus cloud if the layer has a temperature equal or below than −25°C. These temperatures are reached above 8 km in our experimental site almost all the time.

Atmos. Chem. Phys. Discuss., doi:10.5194/acp-2016-458, 2016
Manuscript under review for journal Atmos. Chem. Phys.
Published: 22 June 2016

Atmospheric Chemistry and Physics
Discussions

2.4. Cirrus Cloud Optical Depth, backscattering coefficient profile and lidar ratio determination.

The attenuation of the lidar signal by cirrus clouds can be obtained using the ratio of the range corrected signal at the top and at the cloud base as in (Young, 1995):

$$\frac{S(z_t)}{S(z_b)} = \frac{\beta(z_t)}{\beta(z_b)} e^{-2\int_{z_b}^{z_t} \alpha_p(z')dz'} e^{-2\int_{z_b}^{z_t} \alpha_m(z')dz'} \quad (1)$$

where z_b and z_t are the base and top of cirrus clouds heights, $S(z) = P(z)z^2$ is the range corrected signal. $\beta(z)$ and $\alpha(z)$ are the volumetric backscattering and extinction coefficients, respectively, and each is the sum of a molecular (sub index m) and a particle (sub index p) contribution. Volumetric backscattering and extinction profiles from molecules were derived following Bucholtz (1995). Assuming a negligible aerosol contribution in the atmospheric layers just below and above the cirrus clouds (Young, 1995), we can express the transmittance factor of the lidar equation due to cirrus cloud, T^{cirrus}, as:

$$T^{cirrus} = e^{-2\int_{z_b}^{z_t} \alpha_p(z')dz'} = \frac{S(z_t)}{S(z_b)} \frac{\beta(z_b)}{\beta(z_t)} e^{2\int_{z_b}^{z_t} \alpha_m(z')dz'} \quad (2)$$

And the cirrus optical depth (for an example, see Figure S.2), τ^{cirrus}, as:

$$\tau^{cirrus} = \int_{z_b}^{z_t} \alpha_p(z')dz' = -\frac{1}{2}\ln(T^{cirrus}) \quad (3)$$

The accuracy of this calculation depends mainly on the SNR at the cirrus cloud altitude. However, when the lidar signal is completely attenuated by the cirrus cloud, i.e. the transmission factor goes to zero, it is impossible to obtain the true values of the cirrus top altitude and optical depth. The retrievals, in these cases called apparent values, are necessarily underestimated. Tilting the system by about 5^{o} from the zenith minimizes the effect of the specular reflection on the quasi-horizontal ice crystals.

The backscattering coefficients of cirrus clouds were determined by the Fernald-Klett-Sasano method (Fernald et al., 1972; Klett, 1981; Sasano and Nakane, 1984) for each 5-min averaged profile that has large enough SNR above the cirrus cloud, thus allowing a molecular fit. For retrieving the extinction, however, the Klett method requires a predetermined value for the lidar ratio (LR), which is the ratio between the extinction and backscattering coefficients. Then, integrating the extinction coefficient from the cloud base to cloud top, the cirrus cloud optical depth is obtained (τ_{Klett}^{cirrus}). Following Chen et al. (2002), we estimated the value of LR for every cloud by iterating over the values of LR and comparing the values of τ_{Klett}^{cirrus} with the independent value of the cirrus optical depth obtained from the transmittance method described above (τ^{cirrus}). The cirrus lidar ratio is the one that minimizes the residue: $R(S) = \left(\tau_{Klett}^{cirrus} - \tau^{cirrus}\right)^2$.

The Klett method assumes single scattering, but eventually the received photons could have been scattered by other particles several times before reaching the telescope. This effect named multiple scattering increases the laser transmittance and decreases the real extinction coefficient values. Thus, a correction is needed in our calculation of cirrus optical depth. As explained by Chen et al. (2002), for thin clouds it is possible to neglect the multiple scattering effect, nevertheless, we used their proposed correction for all cirrus clouds detected:

$$\eta = \frac{\tau^{cirrus}}{e^{\tau^{cirrus}}-1}; \quad \tau_{corrected}^{cirrus} = \frac{\tau^{cirrus}}{\eta} \quad (4)$$

3. Results and discussion.

3.1. Frequency of cirrus cloud occurrence.

A total of 13,946 lidar profiles were measured with the presence of cirrus clouds, representing a frequency of occurrence of 67 % of the total number of profiles with good SNR. Figure 2 shows the monthly frequency of occurrence of cirrus clouds in central Amazônia from July 2011 to June 2012, blue solid line. There is a well-defined annual cycle, with maximum values during the months of November, December and March, reaching approximately 85 %, and minimum value in August during the dry season, but with frequencies no lower than a rather high 50 %. In tropical regions, the main mechanisms of cirrus clouds formation are deep convection, large-scale lifting of moist layers, orographic lifting over mountain slopes and "cold trapping" near the tropopause (Sassen et al, 2002). Deep convective clouds generate cirrus clouds while winds in the upper troposphere removes ice crystals of the top of the large convective column, generating the anvil cloud. This cloud remains even after the deep convection cloud dissipation and persist from 0.5 to 3 days (Seifert et al, 2007). Due to the huge amount of deep convection in the Amazon region (Machado et al., 2002; 2014), and the lack of the others formation mechanisms proposed in the literature (Sassen et al., 2002), e.g. baroclinic fronts and lows and orographic lifting, it is expected that cirrus clouds are basically formed by this mechanism. However, it should be noted that small local topographic effects around Manaus can influence the occurrence and intensity of deep convection (Fitzjarrald et al. 2008; Adams et al. 2015). The frequency of deep convection during the rainy season is higher than the dry season, related with the seasonal change of the Intertropical Convergence Zone (ITCZ). The boxplot in Figure 2 show the variability of the daily frequency of occurrence for each month. There is a high dispersion of the daily frequencies, maximum dispersion in August and lowest in November. The monthly cirrus cloud frequency follows the same seasonal pattern as the accumulated precipitation (Figure 2, green line), maximums during the wet months and minimums during dry months. For that reason, we divided the study period in wet (January, February, March and April), dry (June, July, August and September) and transition (May, October, November and December) periods, based on the accumulated precipitation in each month. The average monthly precipitation in each season during the observation period was 314 mm, 114 mm and 206 mm respectively.

The mean wind field on the typical cirrus cloud occurrence altitude (200 hPa) and the precipitation spatial distribution during the dry and wet months from July 2011 to June 2012 are shown in the Figure 3. During wet months (Figure 3, lower panel), the site is inside the South American Monsoon region with great deep convection activity and associated rain ranging from 8 to 14 mm/day on average. Winds at 200 hPa blow from the southeast with about 20 m/s thus allowing the advection of cirrus clouds produced over other parts of the South Atlantic Convergence Zone. As the tropical cirrus can be transported by advection thousands of kilometers (Fortuin et al., 2007), we speculate that during the wet period, the cirrus clouds observed in central Amazonia are a mixture of locally produced and clouds transported by advection from other regions. During the dry period, the convection activity moved to the north over Colombia and Venezuela and the 200 hPa circulation is reversed. Hence, we speculate based on the high level circulation and precipitation, that a great contribution to the cirrus clouds observed during the dry months is the advection from the other regions.

The diurnal cycle of the frequency of cirrus clouds is shown in the Figure 4 for the overall period and different seasons. All curves exhibit a similar pattern with minimum frequency occurrence values around 10 and 14 LT hours. Maximum values are found between 17 and 18 LT, in late afternoon, when values are slightly higher than in the morning. This diurnal variation of cirrus cloud occurrence follows the diurnal cycle of convection and precipitation documented in the literature (e.g. Machado et al., 2002; Silva et al., 2011, Adams et al. 2013). Figure 4 shows also the diurnal cycle of precipitation for wet and dry months during the study period, averaged over an area of 2° x 2° centered on the experimental site. The maximum of the cycle occurs between 13 and 18 LT, both in dry and wet months, similar to Adams et al. (2013). The occurrence of the maximum precipitation in the afternoon coincides with the increase in the cirrus frequency in all seasons.

A larger difference between the maximum and minimum values of the cirrus frequency for the dry months is visible in Figure 4. This can be understood by observing the maximum precipitation rates during this period, six times lower than those of the wet months, and the upper level circulation (Figure 4) that indicates the long range advection. When the frequency of deep convection is greater, close to the site, the cirrus clouds are long-lived and more evenly distributed during the day, which does not occur during the dry months.

3.2. Geometrical, optical and microphysical properties of cirrus clouds.

Table 2 shows the statistics of the properties of cirrus clouds during the study year and different seasons. The overall mean values for the cloud base altitude is 12.7 ± 2.3 km, cloud top is 14.4 ± 2.0 km and geometrical thickness is 1.7 ± 1.5 km. The mean value of the cloud maximum backscattering altitude is 13.2 ± 2.3 km, where the mean temperature is −58 ± 17 °C. The differences between the mean values of the geometrical properties in different seasons are statistically significant. The frequency of occurrence of all cirrus clouds throughout the year was 67 % of the time measurements with good SNR. The seasonal behavior discussed previously is also evident, with higher values of frequency of occurrence during the wet months (82 %) and lower during dry months (55 %). The mean values of the geometrical characteristics are similar, only the thickness is slightly different with 1.9 km (1.6 km) for wet (dry) months. Mean COD values are 0.46 and 0.27 for the wet and dry months, respectively. Although the similarities between the mean values of the characteristics of all cirrus clouds during both seasons there are statistically significant differences between the mean values of the geometrical properties in the different seasons.

Our mean values are similar to those reported by Seifert et al. (2007) in the Maldives (4.1 °N, 73.3 °E): 11.9 ± 1.6 km (base), 13.7 ± 1.4 km (top), 1.8 ± 1.0 km (thickness), 12.8 ± 1.4 km (max. backscatter) and −58 ± 11 °C (temperature at max. backscatter). Reports from subtropical regions also show similar values. Cadet et al. (2003) report for the Reunion Island (21°S, 55°E) cirrus cloud base and top altitudes of 11 km and 14 km, respectively. Antuña and Barja (2006) report to subtropical experimental site (21.4° N, 77.9° W) cirrus cloud base and top altitudes of 11.63 km and 13.77 km, respectively. On the other hand, Sassen and Campbel (2001) show mean values for midlatitude cirrus cloud base/top of 8.79 km/11.2 km, lower as expected than tropical cirrus and an average geometrical thickness of 1.81 km. Some cirrus clouds characteristics reported around the globe are shown in Table 1 for comparison. What stands out is that our measurements over the Amazon show high frequency of occurrence of subvisible cirrus clouds similar or higher than previously reported from ground-based measurements in the Tropics.

The geometrical characteristics of the detected cirrus clouds were examined by means of normalized histograms. Figure 5 shows the results for cloud base and top height, thickness and the corresponding optical depth.

Histograms for the wet and dry months reveal differences. The cirrus clouds top altitude distribution (figure 5b), for instance, shows two peaks in the wet months, one centered in 14.25 km and second centered in 17.75 km, with a local minimum centered in 15.25 km and 16.25 km. On the other hand, for dry months, there is only one peak centered at 15.75 km. The local minimum during wet months occurs at 15.25 km, where a higher value near to maximum is found during dry months.

For the cloud base (figure 5a), the maximum frequency is in an interval of altitudes around 12.25 km. Similar value of frequency is found in other peak centered at 14.75 km, with local minimum in 14.25 km. There is a local maximum centered in 16.25 km during wet months. For the dry months, this last peak disappears, but the other two peaks remains with higher frequency values and with local minimum in 13.75 km. These results suggest different cirrus types with different origins: cirrus formed directly by anvil outflows from cumulonimbus clouds through local convection; in situ formation from slow large scale air ascent; or possible advection from other convective regions. Comstock et al. (2002) proposed two different types of cirrus clouds at Nauru Island in the tropical western Pacific with oceanic conditions: one type (laminar thin cirrus) with cloud base altitude above 15 km and the other (geometrically thicker and more structured cirrus) with base altitude below this value, with different characteristics. Liu and Zipser (2005) used TRMM Precipitation Radar (PR) dataset to trace the deep convection and precipitation throughout the tropical zone, including oceans and continents. The authors showed that only 1.38 % and 0.1% of tropical convective systems, and consequently their generated cirrus clouds reached 14 km and 16.8 km of altitude, respectively. Hence, they suggested that those clouds with bases about 14 km are the thick anvil type cirrus, and the higher, thin cirrus have their bases above this altitude during the entire study period.

Considering these previous results, we suggest that the highest peaks in wet months and the single peak in dry months in cloud base and top histograms have the contribution of cirrus clouds formed far from the site and were transported from large distances. The clouds generated by convective systems can persist in the atmosphere from hours to days if they are slowly lifted (Ackerman et al., 1988; Seifert et al., 2007). Thus, these clouds that ascended and were horizontally transported by long distances are, in general, optically and geometrically thinner and found in upper troposphere and tropical tropopause layer. Our results indeed indicate that these clouds are optically thin. This could be also the reason for which the geometrical thicknesses and optical depth are lower in the dry months see Figure 5 c and d, respectively. We can see that the distribution of the geometrical thickness below 2 km and optical depth below 0.1 in dry months is above the distribution for the wet months.

From the cloud base altitude histogram (Figure 5a), one can note the high values for the frequency of occurrence of cloud base heights between 8.5 km and 9.5 km during wet season. This peak is the second most frequent after the principal one centered at 12.25 km and 14.75 km. This secondary peak is a result of using the cloud-base temperature of −25 C as a criterion for defining cirrus clouds. For this altitude, there is possibly a fraction of mixed phase clouds that are counted inadvertently. The most reliable way of identifying the cloud phase is by measuring the depolarization caused by backscattered light, not available in the present study.

Figure 5d shows the normalized histogram of the cirrus clouds optical depth (COD) for the studied period and just the wet and dry seasons. In this case, the apparent COD values (explained in section 2) were excluded. This histogram shows how the frequency decrease with increases in COD. Moreover, during dry months, the cirrus clouds are optically thinner than during wet months.

A more in-depth analysis of the vertical distribution of cirrus clouds reveals features of different cirrus types, and its relation with COD becomes apparent. Figure 6 shows two-dimensional histograms of cloud optical depth and cirrus cloud top (upper row) and cloud base (lower row) for the wet months (left column) and dry months (right column). During the wet months, there is more dispersion of the values than in the dry months, which we speculate might be associated with a larger variability in the outflow altitude from deep convective clouds. The cloud-base distributions (Figure 6c, d) clearly show that the higher values of COD correspond to lower cloud base, whereas the lower values correspond to higher cloud base. The almost linear decrease is steeper for wet months (Figure 6c) than dry months (Figure 6d), hence, cirrus with the same cloud base altitude are more optically thick during that period. There are two maxima during the dry months suggesting two types of cirrus clouds, those with bases below and those with bases above 13.75 km. The low altitude type has a cloud base at about 12.25 km and COD 0.20, while the high altitude ones, have a base at 14.75 km and subvisible optical depths of 0.01. During wet season, the two groups are much less pronounced and have higher COD. These cirrus clouds types were previously reported for the tropical region by Comstock et al. (2002) and Pace et al. (2003). However, the altitude that separates these two types of clouds over the Amazon (13.75 km) is lower than that reported over Nauru Island in the tropical western Pacific (15 km) by Comstock et al. (2002) and over Mahé Island in the tropical Indian Ocean (14.50 km) by Pace et al. (2003). Moreover, we also identified another group of subvisible clouds with very high cloud base (16.25 km) during the wet months, which is likely above the tropopause.

In the case of cloud top, the relation with COD is not clear. During the dry months (Figure 6b), almost all cirrus clouds tops, regardless of their COD, are found around 16.75 km. During the wet months, the cloud tops are spread from 13 km to 16 km, but all COD values occur at all altitudes. To investigate the role of the tropopause capping on the cirrus vertical development, its altitude was calculated from the ERA Interim dataset (see section 2). The tropopause mean altitudes during the wet, transition and dry periods are 16.5 ± 0.2 km, 16.3 ± 0.3 and 15.9 ± 0.4, respectively.

Figure 7 shows the distribution of the distance from the cloud top and bottom to the tropopause. About 7 % (22 %) of the detected cirrus clouds have cloud base (top) above the tropopause during the wet season, and 6 % (17 %) during the dry season. Most of the cirrus clouds tops are found right below the tropopause inversion (see figure S.3a and S.3b), except during the wet season when they are found from -3 km to +0.5 km. The presence of the cirrus clouds in the tropical tropopause layer is the consequence of the deep and strong convection in the Amazonian region reported previously by Liu and Zipser (2009). Their vertical distribution can then be understood as following. During the wet season, the intensity of deep convection in central Amazonia (as measured with convective available potential energy, water

Atmos. Chem. Phys. Discuss., doi:10.5194/acp-2016-458, 2016
Manuscript under review for journal Atmos. Chem. Phys.
Published: 22 June 2016

vapor convergence, cloud top temperatures) can vary (Machado et al., 2002; Adams et al., 2009, 2013, 2015). Moreover, the tropopause is higher during the wet season (figure S.3c). Hence the cloud tops can be found from 13 km to 18 km, and cloud bases from 9 km to 18 km (figure 6). During the dry season, deep convection is found primarily north of the equator (figure 3), hence the cirrus clouds measured at Manaus are mostly those transported over long distances by the prevailing winds (figure 3). As the cirrus produced northward around the tropopause do not last long, as they cannot be adiabatically lifted (Jensen et al., 1996), they do not reach the measurement site and there is only one maximum near 15 km in the distribution of cloud tops. During these dry months over the Amazon, however, precipitation is still about 100 mm per month. Hence, there is a second type of cirrus clouds (Figure 7a and 6d), which those are produced nearby, and hence are lower and optically thicker.

The statistical characteristics of cirrus clouds above and below 14 km are shown in the Table 2. Mean values of the properties are different for these cloud types. Cirrus clouds above 14 km are geometrical and optically thinnest than clouds below 14 km. There are statistically significant differences between the properties of these two cirrus clouds types and between seasons. Also, there is a seasonal behaviour of the of these cloud types. During wet months the cirrus clouds are higher and optical and geometrically thicker than during the dry months.

The classification of cirrus clouds following Sassen and Cho (1992) shows that 40.0 % of the cirrus clouds measured in our experimental site are subvisible ($\tau < 0.03$), 37.7 % are thin cirrus ($0.03 < \tau < 0.3$) and 22.3 % are opaque cirrus ($\tau > 0.3$). Table 2 shows these values for each season. subvisible cirrus clouds have the highest (lower) fraction during dry (wet) months. Opaque clouds have the highest (lower) fraction during wet (dry) months, which is expected as there is a dominance of newly generated clouds by deep convection columns. This large fraction of optically thin and subvisible cirrus clouds over the Amazon present a challenge for using passive remote sensing from space, such as MODIS. As mentioned by Ackerman et al. (2010), thin cirrus clouds are difficult to detect because of insufficient contrast with the surface radiance. MODIS only detects cirrus with optical depth higher than 0.2 (Ackerman et al., 2008). Therefore, the MODIS's cloud-mask does not include 71 % of cirrus clouds over the Amazon, and likewise, their estimation of aerosol optical depth might be contaminated with these thin cirrus. Aerosol optical depth measurements from AERONET can also be contaminated with thin cirrus clouds. Chew et al. (2011), for instance, estimated a contamination of about 0.034 to 0.060 in AERONET AOD in Singapore, where the cirrus frequency of occurrence is about 34%. Therefore, in our region with much higher cirrus frequency, the AERONET AOD might be more contaminated. Exactly how much contamination from thin cirrus there might be in MODIS and AERONET aerosol products over the Amazon will be the subject of a forthcoming study.

These different types of cirrus clouds measured in central Amazonia, with different formation mechanisms, optical depths and altitude range are expect to be composed of ice crystals of different shapes. One way to gain information is to compute the ratio of the backscatter to the total extinction, the so-called lidar-ratio. As explained in section 2, we are able to find the average lidar-ratio for the detected cirrus clouds using an interactive approach instead of explicitly calculating the extinction from the Raman signal, which would be available only during night-time. Figure 8 shows the histograms of lidar ratio values for cirrus clouds during dry and wet months. The cirrus clouds were divided in three categories, following our previous discussion: those clouds with base above 14 km, top below 14 km and those with top (base) above (below) 14 km. In all case, the most frequent lidar ratios are between 16 sr and 20 sr. There are notable differences only for the distributions for higher clouds (base above 14 km) during dry months, when we observed two types of cirrus (Figure 6). For dry months, there is a large frequency of occurrence of cirrus clouds with lidar ratios around 40 sr. According to the study of Sassen et al. (1989), cirrus clouds composed of thick plates, long columns and thin plates would have lidar ratio values around 11.6 sr, 26.3 sr and 38.5 sr, respectively. Hence, during wet months there is the predominant mixture of thick plates and long columns for all clouds. During dry months, the cirrus clouds that are entirely above 14 km have an important contribution of thin plates. These are long-range transported cirrus, thus the aged ice crystals, will tend to become thinner during the transport.

The mean value of 20.2 ± 7.0 sr is obtained for the whole period and varying less than 1.5 sr for different season months. Pace et al., (2003) showed a distribution to the inverse value of lidar ratio similar to that presented here. They found a mean value of lidar ratio of 19.6 sr for the tropical site of Mahé, Seychelles. Seifert et al.(2007), also for tropical regions report values near to 32 sr. Platt and Diley, (1984) reported the value of 18.2 sr with an error of 20%. The value of the lidar ratio may vary greatly depending on the altitude and composition of cirrus clouds (Goldfarb et al., 2011). For the other latitudes, there are differences between the lidar ratio values examples given in Table 1.

After the analysis of the properties of the cirrus clouds it is interesting to examine the behavior of the variable with the temperature. Figure 9 show the dependence of the geometrical thickness, optical depth and lidar ratios with the cirrus clouds temperature. The plots show temperature uniform intervals of 2.5 °C, and the variables with their mean and standard deviation for each corresponding interval. The upper and middle panels contain the dependence of the geometrical thickness and optical depth with cloud base temperature, respectively. We can see both variables increase at higher temperatures. Values nearly to 3 km of geometrical thickness and 0.9 optical depth correspond to a temperature of −25 °C, decreasing monotonically for lower temperatures in both month's periods. Similar results are reported by Hoareau et al. (2013) and Seifert et al. (2007).

Lower panel in Figure 9 shows the dependence between lidar ratio with mid-level cloud temperature. A slight increase in the lidar ratio values from 15 sr to 24 sr when the temperature decrease up to −70 °C is showed for dry period. During the wet period, the lidar ratio values are between 15 sr and 20 sr in all temperature intervals. Seifert et al. (2007) and Pace et al. (2003) both show the same temperature dependence of the lidar ratio, but with different mean values of lidar ratio. This behavior is an indication of little variation in the microphysical characteristics of observed clouds. Nevertheless, for the dry period, the lidar ratio grows when temperatures are below −75 °C. These temperature intervals correspond to the clouds above 14 km discussed previously. These clouds above 14 km have different ice crystals shapes concluded from the analysis of the right panel from Figure 9.

4. Conclusions.

The ACONVEX site started in 2011 with the goal of continuously monitoring climate relevant cloud properties in central Amazonia. The ground based lidar measurements from July 2011 to June 2012 were used to investigate the geometrical and optical properties of cirrus clouds in the region. An algorithm was developed to search through this dataset with high vertical and temporal resolution and to automatically find the clouds, calculate the particle backscatter, and derive the optical depth and lidar-ratio. The frequency of occurrence during the observation period was 67 %, which is higher than all previous reports in the literature for other tropical regions. This frequency reached 82 % during the wet months (January, February, March and April), but decreased to 55 % during the dry months (June, July, August, and September). The analysis of high-level circulation and precipitation during the dry months indicate that advection from the northern regions is likely the main source of these cirrus. Whilst during the wet period, there was a mixture of locally produced and advected clouds. However, the diurnal cycle of the frequency of cirrus clouds showed a minimum around 12h LT and maximum around 18h LT, following the diurnal cycle of the precipitation for both seasons.

The geometrical, optical and microphysical characteristics of cirrus clouds measured in the present study were consistent and in agreement with other reports from tropical regions. The mean values were 12.7 ± 2.3 km (base), 14.4 ± 2.0 km (top), 1.7 ± 1.5 km (thick), 0.36 (optical depth) and 20.2 sr (lidar ratio). With the exception of the optical depth and lidar ratio, these mean values are similar to those found during the wet, transition and dry periods. Cirrus clouds were found at temperatures up to −90 °C and 7 % of the cirrus were above the tropopause level or in the tropical tropopause layer. The role of these clouds in wetting or drying the stratosphere was left for another study.

By simultaneously analyzing cloud altitude and COD, it was found that cirrus clouds during the dry months are optically thinner and lower in altitude than those during the wet period. Moreover, the higher values of COD correspond to lower cloud base, whereas the lowest values, to higher cloud base. The almost linear decrease is steeper for wet months than dry months, hence, cirrus with the same cloud base altitude are more optically thick during wet season. The statistical distribution of altitude and COD suggested the presence of two cloud types as expected. The first is located above 14 km with COD ~ 0.02, and the second type at lower altitudes with COD ~ 0.2. A third type, not previously reported, was identified during the wet season, between 16 and 18 km with COD ~ 0.005. Cirrus clouds above 14 km were geometrically and optically thinner than those below, but have higher lidar ratios.

For the first time, the lidar ratio of cirrus clouds was obtained for this region. The mean lidar ratio was 20.2 ± 7.0 sr, indicating a mixture of thick plates and long columns ice crystals, in agreement with other reports from the tropical regions. The statistical distribution of lidar ratios measured in the different seasons is the same, and they also do no vary with the temperature (altitude) of the cirrus clouds, indicating that these clouds are well mixed in the vertical. It was observed, however, that the distribution of the lidar ratio for clouds above 14 km during dry months shows a secondary peak around 40 sr, suggesting a different crystal shape like thin plates. From all cirrus clouds observed, 40 % were classified as subvisible (COD < 0.03), 38 % were as thin (0.03 < COD < 0.3) and 22 % as opaque (COD > 0.3). During the dry months, the suvisible cirrus clouds reached a maximum of 46 %, while opaque cirrus has their maximum during wet months. These values are characteristic for our region and slightly different from measurements in other tropical regions. The central Amazon has a high frequency of cirrus clouds in general, and a large fraction of subvisible cirrus clouds. Therefore, the aerosol optical depth determined by sun-photometers and satellite based sensor in this region might be contaminated with the COD of these thin clouds. Future work must be conducted in order to evaluate how large this contamination might be over the Amazon.

5. Acknowledgements

We thank the researcher David K Adams from UNAM for reviews and valuable comments to improve the paper content. We acknowledge the financial support from CAPES project A016_2013 on the program Science without Frontiers, FAPESP Research Program on Global Climate Change under research grants 2008/58100-1, 2009/15235-8, 2012/16100-1, 2013/50510-5, and 2013/05014-0. Maintenance and operation of the instruments at the experimental site would not have been possible without the institutional support from EMBRAPA. We thank INPA, The Brazilian Institute for Research in Amazonia and the LBA Central office for logistical support. Special thanks to Marcelo Rossi, Victor Souza and Jocivaldo Souza at Embrapa, and to Ruth Araujo, Roberta Souza, Bruno Takeshi and Glauber Cirino from LBA.

6. References

Ackerman, S., Holz, R., Frey, R., and Eloranta, E.: Cloud Detection with MODIS: Part II Validation, J Atmos Oceanic Tech, 25(1073-1086), doi:DOI:10.1175/2007JTECHA1053.1, 2008.

Ackerman, S., Frey, R., Strabala, K., Liu, Y., Gumley, L., Baum, B., Menzel, P.: Discriminating Clear-Sky From Cloud With MODIS. Algorithm Theoretical Basis Document (MOD35). ATBD Version 6.1. October 2010. 2010.

Adams, D. K., Souza, E., and Costa, A.: Moist Convection in Amazonia: Implications for Numerical Modeling (in Portuguese). Revista Brasileira de Meteorologia, 13, 168-178, 2009.

Adams, D. K., Gutman, S. I., Holub, K. L., and Pereira, D. S.: GNSS observations of deep convective time scales in the Amazon. Geophysical Research Letters, 40, 2818-2823, 2013.

Adams, D. K., Fernandes, R. M. S., Holub, K. L., Gutman, S. I., Barbosa, H. M. J., Machado, L. A.T., Calheiros, A. J. P., Bennett, R. A., Kursinski, E. R., Sapucci, L. F., DeMets, C., Chagas, G. F. B., Arellano, A., Filizola, N., Amorim Rocha, A. A., Araújo Silva, R., Assunção, L. M. F., Cirino, G. G., Pauliquevis, T., Portela, B. T. T., Sá, A., de Sousa, J. M., and Tanaka, L. M. S: The Amazon Dense GNSS Meteorological Network: A New Approach for Examining Water Vapor and Deep Convection Interactions in the Tropics. Bull. Amer. Meteor. Soc., 96, 2151–2165, 2015.

Antuña, J. C. and Barja, B.: Cirrus cloud optical properties measured with lidar in Camagüey, Cuba, Óptica Pura y Aplicada, 39, 11–16, 2006.

Arraut, J.M., Nobre, C.A., Barbosa, H.M.J., Marengo J.A., and Obregon, G.: Aerial Rivers and Lakes: looking at large scale moisture transport, its relation to Amazonia and to Subtropical Rainfall in South America, J. Climate, 25, pp. 543-556, doi: 10.1175/2011JCLI4189.1, 2012.

Baars, H., Ansmann, A., Althausen, D., Engelmann, R., Heese, B., Müller, D., Artaxo, P., Paixao, M., Pauliquevis, T., and Souza, R.: Aerosol profiling with lidar in the Amazon Basin during the wet and dry season, J. Geophys. Res., 117, D21201, 2012.doi:10.1029/2012JD018338, 2012.

Barja, B., Aroche, R.: Cirrus clouds at Camagüey, Cuba, Proceedings of the SPARC 2000, 2001.

Atmos. Chem. Phys. Discuss., doi:10.5194/acp-2016-458, 2016
Manuscript under review for journal Atmos. Chem. Phys.
Published: 22 June 2016

Atmospheric Chemistry and Physics
Open Access
Discussions

Barja, B. and Antuña, J. C.: The effect of optically thin cirrus clouds on solar radiation in Camagüey, Cuba, Atmos. Chem. Phys., 11, 8625–8634, doi:10.5194/acp-11-8625-2011, 2011.

Barbosa, H. M. J., Pauliquevis, T., Adams, D. K., Artaxo, P., Cirino, G., Barja, B., Correia, A., Gomes, H., Gouveia, D. A., Padua, M. B., Rosario, N. M. E., Souza, R. A. F., Santos, R. M. N., Sapucci, L., and Portela, B. T.: ACONVEX—Aerosols, Clouds, cONvection, Experiment—A new site in central Amazonia for long term monitoring of aerosol-clouds-convection interactions. In: AMS 95th Annual Meeting Proceedings – Phoenix, Arizona, January 2015, 2015.

Barbosa, H. M. J., Barja, B., Pauliquevis, T., Gouveia, D. A., Artaxo, P., Cirino, G. G., Santos, R. M. N., and Oliveira, A. B.: A permanent Raman lidar station in the Amazon: description, characterization, and first results, Atmos. Meas. Tech., 7, 1745-1762, doi:10.5194/amt-7-1745-2014, 2014.

Boucher, O., Randall, D., Artaxo, P., Bretherton, C., Feingold, G., Forster, P., Kerminen, V.-M., Kondo, Y., Liao, H., Lohmann, U., Rasch, P., Satheesh, S.K., Sherwood, S., Stevens, B., and Zhang, X.Y.: Clouds and Aerosols. In: Climate Change 2013: The Physical Science Basis. Contribution of Working Group I to the Fifth Assessment Report of the Intergovernmental Panel on Climate Change [Stocker, T.F., D. Qin, G.-K. Plattner, M. Tignor, S.K. Allen, J. Boschung, A. Nauels, Y. Xia, V. Bex and P.M. Midgley (eds.)]. Cambridge University Press, Cambridge, United Kingdom and New York, NY, USA, 2013.

Bucholtz, A.: Rayleigh-scattering calculations for the terrestrial atmosphere, Applied Optics 34, 2765–2773, 1995.

Cadet, B., Goldfarb, L., Faduilhe, D., Baldy, S., Giraud, V., Keckhut, P., and Réchou, A., A sub-tropical cirrus clouds climatology from Reunion Island (21°S, 55°E) lidar data set, Geophys. Res. Lett., 30(3), 1130, doi:10.1029/2002GL016342, 2003.

Chen, W.; Chiang, C.; Nee, J.: Lidar ratio and depolarization ratio for cirrus clouds. Applied Optics, v. 41, n. 30, p. 6470 6476, 2002.

Chew B, Campbell J, Reid J, Giles D, Welton E, Salinas S, Liew S.: Tropical cirrus cloud contamination in sun photometer data. Atmospheric Environment;45 (37):6724-6731, 2011.

Comstock, J. M., Ackerman, T. P., and Mace, G. G.: Ground-based lidar and radar remote sensing of tropical cirrus clouds at Nauru Island: Cloud Statistics and radiative impacts, J. Geophys. Res.,107, 4714, doi:10.1029/2002JD002203, 2002.

Dupont, J.-C., Haeffelin, M., Morille, Y., Noël, V., Keckhut, P., Winker, D., Comstock, J., Chervet, P., and Roblin, A.: Macrophysical and optical properties of midlatitude cirrus clouds from four ground-based lidars and collocated CALIOP observations, J. Geophys. Res., 115, D00H24, doi:10.1029/2009JD011943, 2010.

Elouragini, S., and Flamant, P. H.: Iterative method to determine an averaged backscatter-to-extinction ratio in cirrus clouds", Applied Optics, 35, Issue 9, pp. 1512-1518, 1996.

FCM-H3-1997: Rawinsonde and Pibal Observations, Federal Meteorological Handbook No. 3, http://www.ofcm.gov/fmh3/text/rawinson.htm, 1997

Fernald, F. G., Herman, B. M. and Reagan, J. A.: Determination of aerosol height distribution by lidar, Appl. Opt., 11, 482–489, 1972.

Atmos. Chem. Phys. Discuss., doi:10.5194/acp-2016-458, 2016
Manuscript under review for journal Atmos. Chem. Phys.
Published: 22 June 2016

Fitzjarrald, D. R., Sakai, R. K., Moraes, O. L. L., de Oliveira, R. C., Acevedo, O. C., Czikowsky, M. J., and Beldini, T.: Spatial and temporal rainfall variability near the Amazon-Tapajós confluence. J. Geophys. Res., 113, G00B11, doi:10.1029/2007JG000596, 2008.

Fortuin, J. P. F., Becker, C. R., Fujiwara, M., Immler, F., H. M. Kelder, Scheele, M. P., and Schrems, O., Verver, G. H. L.: Origin and transport of tropical cirrus clouds observed over Paramaribo, Suriname (5.8°N, 55.2°W), J. Geophys. Res., 112, D09107, doi:10.1029/2005JD006420, 2007.

Giannakaki, E., Balis, D. S., Amiridis, V., and Kazadzis, S.: Optical and geometrical characteristics of cirrus clouds over a Southern European lidar station, Atmos. Chem. Phys., 7, 5519–5530, doi:10.5194/acp-7-5519-2007, 2007.

Goldfarb, L., Keckhut, P., Chanin, M.-L., and Hauchecorne, A.: Cirrus climatological results from lidar measurements at OHP (44° N, 6° E), Geophys. Res. Lett., 28, 1687–1690, 2001.

Hoareau, C., Keckhut, P., Noel, V., Chepfer, H., and Baray, J.-L.: A decadal cirrus clouds climatology from ground-based and spaceborne lidars above the south of France (43.9° N–5.7° E), Atmos. Chem. Phys., 13, 6951–6963, doi:10.5194/acp-13-6951-2013, 2013.

Hogan, R. J., and Kew, S. F.: A 3D stochastic cloud model for investigating the radiative properties of inhomogeneous cirrus clouds. Q. J. R. Meteorol. Soc., 131, 2585-2608, 2005.

Hong, G., Heygster, G., Miao, J., and Kunzi, K.: Detection of tropical deep convective clouds from AMSU-B water vapor channels measurements, J. Geophys. Res., 110, D05205, doi:10.1029/2004JD004949, 2005.

Huffman, G.J., Adler, R.F., Bolvin, D.T., Gu, G., Nelkin, E.J., Bowman, K.P., Hong, Y., Stocker, E.F., and Wolff, D.B.,: The TRMM multi-satellite precipitation analysis: quasi-global, multi-year, combined-sensor precipitation estimates at fine scale. J. Hydrometeorol. 8 (1), 38–55, 2007.

Immler, F. and Schrems, O.: LIDAR measurements of cirrus clouds in the northern and southern midlatitudes during INCA (55° N, 53° S): A comparative study, Geophys. Res. Lett., 29, 1809, doi:10.1029/2002GL015076, 2002a.

Immler, F., and Schrems, O.: Determination of tropical cirrus properties by simultaneous LIDAR and radiosonde measurements, Geophys. Res. Lett., 29/23, 4, doi:10.1029/2002GL015076, 2002b.

Jensen, E. J., Toon, O. B., Selkirk, H. B., Spinhirne, J. D., and Schoeberl, M. R.: On the formation and persistence of subvisible cirrus clouds near the tropical tropopause, J. Geophys. Res., 101(D16), 21361–21375, doi:10.1029/95JD03575, 1996.

Jiang, J; H., Su, H., Zhai, Ch., Shen, T. J., Wu, T., Zhang, J., Cole, J. N. S., von Salzen, K., Donner, L. J., Seman, Ch., Del Genio, A., Nazarenko, L. S., Dufresne, J.-L., Watanabe, M., Morcrette, C., Koshiro, T., Kawai, H., Gettelman, A., Millán, L., Read, W.G., Livesey, N. J., Kasai, Y., and Shiotani, M.: Evaluating the Diurnal Cycle of Upper-Tropospheric Ice Clouds in Climate Models Using SMILES Observations. J. Atmos. Sci., 72, 1022–1044. doi:10.1175/JAS-D-14-0124.1, 2015.

Kärcher, B.: Cirrus clouds in the tropical tropopause layer: Role of heterogeneous ice nuclei, Geophys. Res. Lett., 31, L12101, doi:10.1029/2004GL019774, 2004.

Atmos. Chem. Phys. Discuss., doi:10.5194/acp-2016-458, 2016
Manuscript under review for journal Atmos. Chem. Phys.
Published: 22 June 2016

Khvorostyanov, V. I., and Sassen, K.: Microphysical processes in cirrus and their impact on radiation A Mesoscale Modeling Perspective, in Cirrus ed D Lynch, K Sassen, D O C Starr and G Stephens (Oxford: Oxford University Press) pp 397–432, 2002.

Kim, Y., Kim, S.-W., Kim, M.-H. and Yoon, S.-C.: Geometric and optical properties of cirrus clouds inferred from three-year ground-based lidar and CALIOP measurements over Seoul, Korea, Atmospheric Research, 139, 27-35, 2014.

Klett, J.D.: Stable analytical inversion solution for processing lidar returns. Appl. Opt. 20(2), 211–220, 1981.

Lakkis, G.S., Lavorato, M., and Canziani, O.P.: Monitoring cirrus clouds with lidar in the Southern Hemisphere: a local study over Buenos Aires. 1. Tropopause heights. Atmos. Res. 92 (1), 18–26, 2009.

Lin, L., Fu, Q., Zhang, H., Su, J., Yang, Q., and Sun, Z.: Upward mass fluxes in tropical upper troposphere and lower stratosphere derived from radiative transfer calculations, J. Quant. Spectrosc. Radiat. Transfer, 117, 114–122, 2013.

Liou, K. N.: Influence of cirrus clouds on weather and climate processes: A global perspective. Mon. Wea. Rev., 114, 1167–1199, 1986.

Liu, C., and Zipser, E. J.: Implications of the day versus night differences of water vapor, carbon monoxide, and thin cloud observations near the tropical tropopause, J. Geophys. Res., 114, D09303, doi:10.1029/2008JD011524, 2009.

Lynch, D. K., Sassen, K., Starr, D. O., and Stephens, G.: Cirrus. Oxford University Press, 480 pp., 2002.

Machado, L.A.T., Laurent, H., and Lima, A.A.: Diurnal march of the convection observed during TRMM-WETAMC/LBA, J. Geophys. Res., 107(D20), 8064, doi:10.1029/2001JD000338, 2002.

Machado, L.A.T.; Laurent, H.; Dessay, N.; Miranda, I.: Seasonal and diurnal variability of convection over the Amazonia - A comparison of different vegetation types and large scale forcing. Theoretical and Applied Climatology, 78, 61-77, doi: 10.1007/s00704-004-0044-9. 2004.

Machado, L.A.T., Silva Dias, M.A.F., Morales, C., Fisch, G., Vila,D., Albrecht, R., Goodman, S.J., Calheiros, A.J.P., Biscaro, T., Kummerow, C.,Cohen, J., Fitzjarrald, D., Nascimento, E.L., Sakamoto, M.S., Cunningham, C., Chaboureau, J. –P., Petersen, W.A., Adams, D.K., Baldini, L., Angelis, C.F., Sapucci, L.F., Salio, P., Barbosa, H.M.J., Landulfo, E., Souza, R.A.F., Blakeslee, R.J., Bailey, J., Freitas, S., Lima, W.F.A., Tokay, A.: THE CHUVA PROJECT: how does convection vary across Brazil? Bull. Am. Meteor. Soc., 1365–1380, doi:10.1175/BAMS-d-13-00084.1, 2014.

Martin, S. T., Artaxo, P., Machado, L. A. T., Manzi, A. O., Souza, R. A. F., Schumacher, C., Wang, J., Andreae, M. O., Barbosa, H. M. J., Fan, J., Fisch, G., Goldstein, A. H., Guenther, A., Jimenez, J. L., Pöschl, U., Silva Dias, M. A., Smith, J. N., and Wendisch, M.: Introduction: Observations and Modeling of the Green Ocean Amazon (GoAmazon2014/5), Atmos. Chem. Phys., 16, 4785-4797, doi:10.5194/acp-16-4785-2016, 2016.

Nazaryan, H., McCormick, M. P., and Menzel, W. P.: Global characterization of cirrus clouds using CALIPSO data, J. Geophys. Res., 113, D16211, doi:10.1029/2007JD009481, 2008.

Atmos. Chem. Phys. Discuss., doi:10.5194/acp-2016-458, 2016
Manuscript under review for journal Atmos. Chem. Phys.
Published: 22 June 2016

Pace, G., Cacciani, M., di Sarra, A., Fiocco, G., and Fuà, D.: Lidar observations of equatorial cirrus clouds at Mahé Seychelles, J. Geophys. Res., 108(D8), 4236, doi:10.1029/2002JD002710, 2003.

Pandit, A. K., Gadhavi, H. S., Venkat Ratnam, M., Raghunath, K., Rao, S. V. B., and Jayaraman, A,: Long-term trend analysis and climatology of tropical cirrus clouds using 16 years of lidar data set over Southern India. Atmos. Chem. Phys., 15, 13833–13848, doi:10.5194/acp-15-13833-2015, 2015

Quante, M., and Starr, D. O'C.: Dynamical processes in cirrus clouds: Review of observational results. Chapter 17 in: D. Lynch, K. Sassen, D.O'C. Starr, G. Stephens (eds.): Cirrus. Oxford University Press, New York, 346-374, 2002.

Randel, W. J. and Jensen, E. J.: Physical processes in the tropical tropopause layer and their roles in a changing climate, Nat. Geosci, 6, 169–176, doi:10.1038/ngeo1733, 2013.

Sasano Y., and Nakane H.: Significance of the extinction/backscatter ratio and the boundary value term in the solution for the two-component lidar equation", Appl. Opt., vol. 23, 11–13, 1984.

Sassen, K., Starr, D. O'C., and Uttal, T.: Mesoscale and Microscale Structure of Cirrus Clouds: Three Case Studies, J of the Atmos. Sci. 46:3, 371-396, 1989.

Sassen, K. and Campbell, J. R.: A midlatitude cirrus cloud climatology from the facility for atmospheric remote sensing. Part I: Macrophysical and synoptic properties, J. Atmos. Sci., 58, 481–496, 2001.

Sassen, K.: Cirrus Clouds. A Modern Perspective, In Cirrus D. Lynch, K. Sassen, D. O´C Starr, and G. Stephens Eds., Oxford University Press, 136-146, 2002.

Sassen, K., Wang, Z., and Liu, D.: Global distribution of cirrus clouds from CloudSat/Cloud-Aerosol Lidar and Infrared Pathfinder Satellite Observations (CALIPSO) measurements, J. Geophys. Res., 113, D00A12, doi:10.1029/2008JD009972, 2008.

Sassen, K., Wang, Z., and Liu, D.: Cirrus clouds and deep convection in the tropics: Insights from CALIPSO and CloudSat, J. Geophys. Res., 114, D00H06, doi:10.1029/2009JD011916, 2009.

Seifert, P.; Ansmann, A.; Muâller, D.; Wandinger, U.; Althausen, D.; Heymsfield, A. J.; Massie, S. T.; Schmitt, C.: Cirrus optical properties observed with lidar, radiosonde and satellite over the tropical indian ocean during the aerosol-polluted northeast and clean maritime southwest monsoon. J. Geophys. Res., v. 112, p. D17205, 2007.

Silva, V. B. S., Kousky, V. E., and Higgins, R. W.: Daily Precipitation Statistics for South America: An Intercomparison between NCEP Reanalyses and Observations. J. Hydrometeorol., 12, 101-117. DOI: 10.1175/2010JHM1303.1, 2011.

Starr, D. O'C., and Quante, M.: Dynamical processes in cirrus clouds: Concepts and models. Chapter 18 in: D. Lynch, K. Sassen, D.O'C. Starr, G. Stephens (eds.): Cirrus. Oxford University Press, New York, 375-396, 2002.

Stubenrauch, C. J., Chédin, A., Rädel, G., Scott, N. A., and Serrar, S.: Cloud Properties and Their Seasonal and Diurnal Variability from TOVS Path-B. J. Climate, 19, 5531–5553, 2006.

Tanaka, L. M. d. S., Satyamurty, P., and Machado, L. A. T.: Diurnal variation of precipitation in central Amazon Basin. Int. J. Climatol. 34, 3574–3584, DOI: 10.1002/joc.3929, 2014.

Atmos. Chem. Phys. Discuss., doi:10.5194/acp-2016-458, 2016
Manuscript under review for journal Atmos. Chem. Phys.
Published: 22 June 2016

Thorsen, T. J., Qiang, F., and Comstock, J. M.: Comparison of the CALIPSO satellite and ground-based observations of cirrus clouds at the ARM TWP sites, J. Geophys. Res., 116, D21203, doi:10.1029/2011JD015970, 2011.

Wang, T., and Dessler, A. E.: Analysis of cirrus in the tropical tropopause layer from CALIPSO and MLS data: A water perspective, J. Geophys. Res., 117, D04211, doi:10.1029/2011JD016442, 2012.

Wendisch, M., et al.: The ACRIDICON–CHUVA campaign: Studying tropical deep convective clouds and precipitation over Amazonia using the new German research aircraft HALO. Bull. Am. Met. Soc., accepted, doi:10.1175/BAMS-D-14-00255.1, 2016

Wylie, D. P., Jackson, D. L., Menzel, W. P., andBates, J. J.: Trends in global cloud cover in two decades of HIRS observations. J. Climate, 18, 3021–3031, 2005.

Yang, P., Hong, G., Dessler, A. E., Ou, S. C., Liou, K. N., Minnis, P., and Hashvardhan,: Contrails and induced cirrus: Optics and radiation. Bull. Amer. Meteor. Soc., 91, 473–478, 2010a.

Yang, Q., Fu, Q., and Hu, Y.: Radiative impacts of clouds in the tropical tropopause layer, J. Geophys. Res., 115, D00H12, doi:10.1029/2009JD012393, 2010b.

Young, S.: Analysis of lidar backscatter profiles in optically thin cirrus, Appl. Opt., 34, 7019–7031, 1995.

Zerefos, C. S., Eleftheratos, K., Balis, D. S., Zanis, P., Tselioudis, G., and Meleti, C.: Evidence of impact of aviation on cirrus cloud formation, Atmos. Chem. Phys., 3, 1633–1644, doi:10.5194/acp-3-1633-2003, 2003.

Atmos. Chem. Phys. Discuss., doi:10.5194/acp-2016-458, 2016
Manuscript under review for journal Atmos. Chem. Phys.
Published: 22 June 2016

Atmospheric Chemistry and Physics
Open Access
Discussions

Tables:

Table 1. Summary of some recent cirrus clouds studies based on at least a few months of ground-based lidar observations in the tropics and mid-latitudes. The first columns show the period of study and laser wavelength (nm) for each site location, for which more than one study might be available. The cirrus characteristics are those reported by the different authors, which might include: base and top height (km), thickness (km), base and top temperature (°C), frequency of occurrence (%) and lidar-ratio (sr).

Measurement site	Location	Period of study	Wave length [nm]	Average values									
				Height [km]			Temp. [°C]		Frequency [%]		LR[sr]	
				Base	Top	Thick.	Base	Top	SVC	Thin		
Salt Lake City, Utah, USA	40.8°N 111.8°W	1986 to 1996	694	8.8	11.2	1.8	−34.4	−53.9	50	-		Sassen and Campbel (2001)
Haute Prov., France	43.9°N 5.7°E	1997 to 2007	532/1064	9.3	10.7	1.4			38		18.2	Goldfarb et al. (2001) Hoareau et al. (2013)
Thessaloniki, Greece	40.6°N 22.9°E	2000 to 2006	355/532	8.6	11.7	2.7	−38	−65		57	30	Giannakaki et al. (2007)
Seoul, South Korea	37°N, 127°E	2006 to 2009	532/1064	8.8	10.6						20	Kim et al. (2009)
Buenos Aires, Argentina	34.6 °S, 58.5 °W	2001 to 2005	532	9.6	11.8	2.4		−64.5				Lakkis et al.(2008)
Reunion Island	21°S, 55°E	1996 to 2001	532	11	14				65		18.3	Cadet et al. (2003)
Camagüey, Cuba	21.4° N, 77.9° W	1993 to 1998	532	11.6	13.8				25		10	Antuña and Barja, (2006)
Gadanki, India	13.5 N, 79.2 E	1998 to 2013	532	13.0	15.3	2.3		−65	52	36	25	Pandit et al., (2015)
Hulule. Maldives	4.1°N, 73.3°E	1999, 2000	532	11.9	13.7	1.8	−50	−65	15	49	32	Seifert et al. (2007)
Mahe´, Seychelles	4.4 °S, 55.3 °E	Feb-Mar 1999	532			0.2-2.0					19	Pace et al., (2003)
Nauru Island	0.5 °S, 166.9 °E	Apr-Nov 1999	532	~14	~16							Comstock et al. (2002)

Atmos. Chem. Phys. Discuss., doi:10.5194/acp-2016-458, 2016
Manuscript under review for journal Atmos. Chem. Phys.
Published: 22 June 2016

Table 2. Mean cirrus cloud properties and standard deviation in parenthesis for all cirrus clouds, for cirrus clouds above and below 14 km and cirrus clouds with base below and top above 14 km. These cloud properties are also informed to total time of observation, wet, transition and dry seasons

All Cirrus Clouds	**Total**	**Wet**	**Transition**	**Dry**
Frequency of Occurrence [%]	67.2	82.2	79.4	55.5
Base Altitude [km]	12.7 (2.3)	12.7 (2.6)	12.5 (2.4)	12.8 (2.1)
Top Altitude [km]	14.4 (2.0)	14.5 (2.2)	14.3 (2.2)	14.4 (1.8)
Thickness [km]	1.7 (1.5)	1.9 (1.6)	1.8 (1.4)	1.6 (1.4)
Cloud Optical Depth	0.36 (1.20)	0.46 (1.49)	0.38 (1.22)	0.27 (0.90)
Max Backscatter Altitude [km]	13.2 (2.3)	13.2 (2.5)	13.0 (2.4)	13.3 (2.0)
Temperature Max. Back. Alt. [°C]	-58.1 (16.9)	-58.0 (18.2)	-56.3 (18.6)	-59.1 (14.8)
Lidar Ratio [sr]	20.2 (7.0)	18.5 (6.5)	19.4 (6.3)	21.3 (7.2)
Subvisual Cirrus [%]	40.0	36.4	33.9	46.0
Thin Cirrus [%]	37.7	37.0	41.7	36.2
Opaque Cirrus [%]	22.3	26.6	24.4	17.7
Cirrus Clouds with Base > 14 km				
Fraction of all cirrus [%]	31.8	32.0	28.7	33.2
Base Altitude [km]	15.4 (1.0)	15.7 (1.1)	15.5 (1.0)	15.2 (0.8)
Top Altitude [km]	16.2 (0.9)	16.6 (0.9)	16.4 (0.9)	15.9 (0.8)
Thickness [km]	0.8 (0.6)	1.0 (0.8)	1.0 (0.7)	0.7 (0.4)
Cloud Optical Depth	0.03 (0.06)	0.04 (0.07)	0.04 (0.07)	0.02 (0.04)
Lidar Ratio [sr]	22.9 (9.5)	20.2 (8.7)	21.7 (9.0)	25.5 (9.7)
Cirrus Clouds with Top < 14km				
Fraction of all cirrus [%]	38.0	38.8	41.9	35.3
Base Altitude [km]	10.8 (1.5)	10.7 (1.5)	10.5 (1.5)	11.2 (1.3)
Top Altitude [km]	12.3 (1.4)	12.3 (1.4)	12.1 (1.3)	12.5 (1.3)
Thickness [km]	1.5 (1.2)	1.6 (1.2)	1.6 (1.2)	1.3 (1.0)
Cloud Optical Depth	0.50 (1.70)	0.67 (2.09)	0.55 (1.64)	0.32 (1.28)
Lidar Ratio [sr]	20.0 (6.7)	19.3 (7.7)	18.9 (6.2)	20.5 (6.4)
Cirrus Clouds with Base< 14km and Top>14 km				
Fraction of all cirrus [%]	30.2	29.2	29.3	31.5
Base Altitude [km]	12.2 (1.4)	11.2 (1.5)	12.3(1.3)	12.3 (1.3)
Top Altitude [km]	15.2 (0.9)	15.3 (1.0)	15.3 (0.9)	15.0 (0.7)
Thickness [km]	3.0 (1.7)	3.3 (1.9)	2.9 (1.5)	2.8 (1.5)
Cloud Optical Depth	0.55 (0.99)	0.70 (1.19)	0.49 (1.01)	0.47 (0.78)
Lidar Ratio [sr]	19.7 (6.3)	18.0 (5.5)	19.1 (5.6)	20.9 (6.7)

Atmos. Chem. Phys. Discuss., doi:10.5194/acp-2016-458, 2016
Manuscript under review for journal Atmos. Chem. Phys.
Published: 22 June 2016

Atmospheric Chemistry and Physics
Open Access
Discussions

Figures:

Figure 1. Location of the experimental site (2.89°S 59.97°W) is shown, 30 km upwind from downtown Manaus-AM, Brazil.

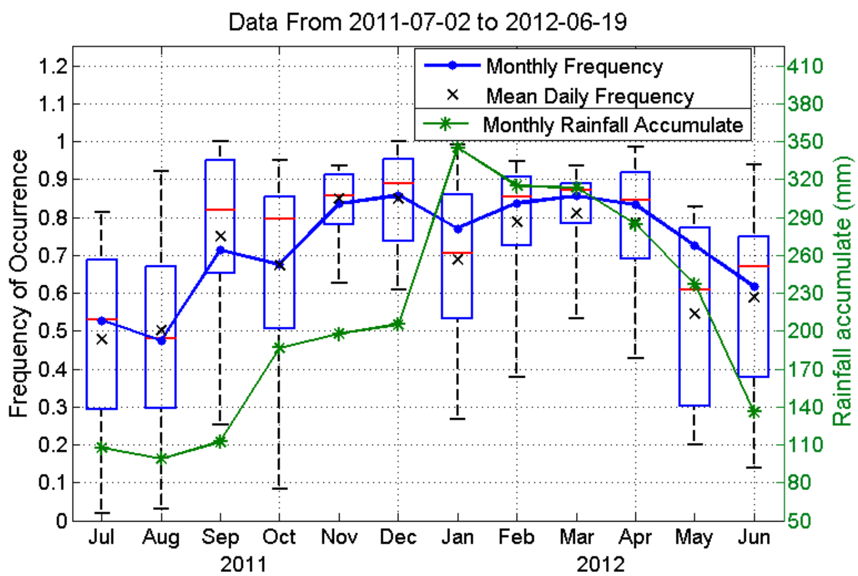

Figure 2. Monthly frequency of occurrence of cirrus clouds from July 2011 to June 2012 (blue line). Red dashes (black x) in the boxplots are the median (mean) of the daily frequency in each month. The edges of the boxes are the 25th and 75th percentiles, and the whiskers extend to the most extreme daily values. Accumulated rainfall is shown in green on the right axis. Data is from TRMM 3B42 version 7.

Atmos. Chem. Phys. Discuss., doi:10.5194/acp-2016-458, 2016
Manuscript under review for journal Atmos. Chem. Phys.
Published: 22 June 2016

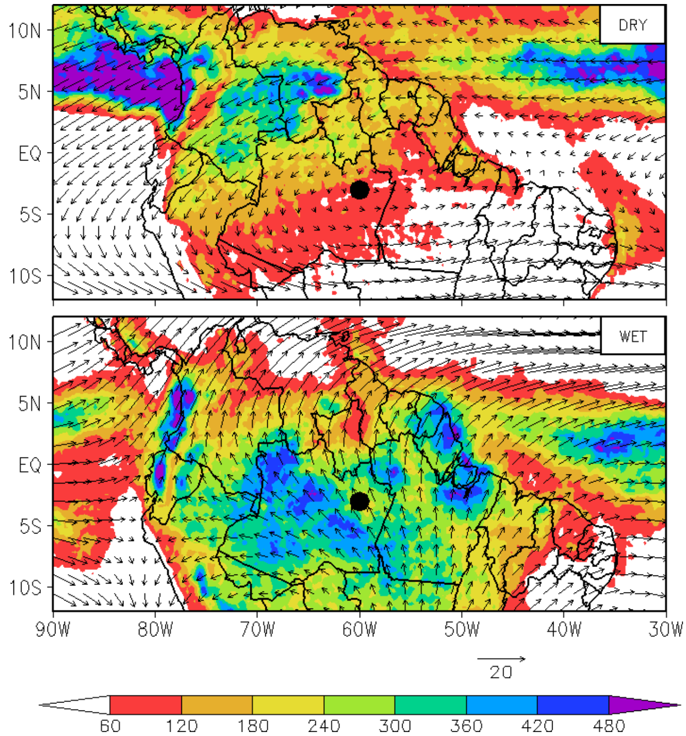

Figure 3. Mean precipitation (colors, mm/day) from the TRMM 3B42 version 7 and mean wind field (vectors, m/s) at 200 hPa from ECMWF ERA Interim reanalysis are shown for the average dry months (JJAS) and wet months (JFMA), between July/2011 and June/2012. The experimental site location is marked with a black dot.

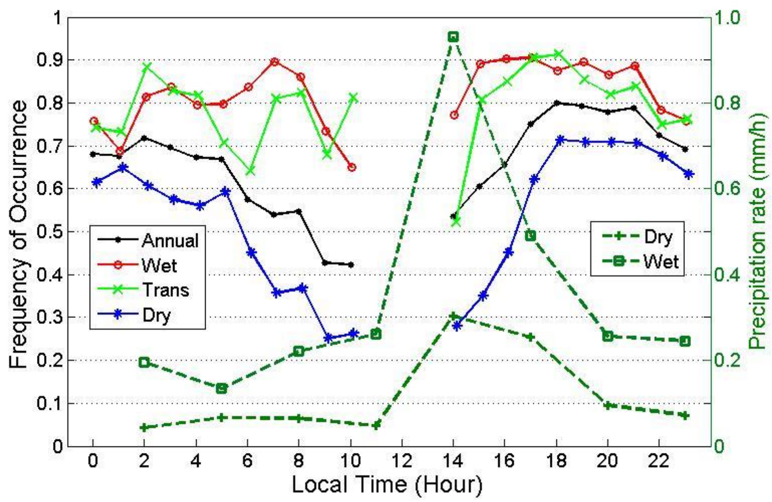

Figure 4. Diel cycles of the hourly frequency of occurrence of cirrus clouds are shown for the annual, wet, transition and dry periods. Mean precipitation rate (mm/h) over an area of 2°× 2°centered in the site is shown in dashed lines for the Dry (+) and wet (☐) periods. Data is from TRMM version 7.

Atmos. Chem. Phys. Discuss., doi:10.5194/acp-2016-458, 2016
Manuscript under review for journal Atmos. Chem. Phys.
Published: 22 June 2016

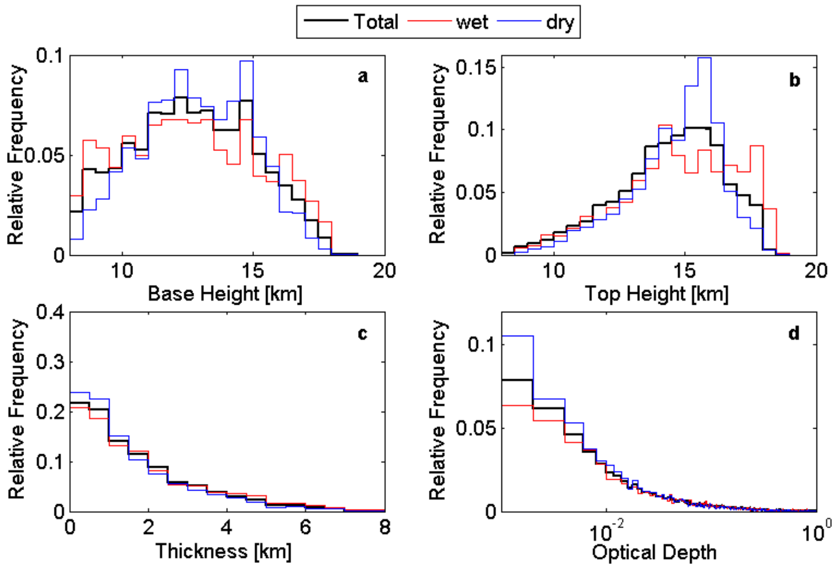

Figure 5. Panels show the normalized histograms of (a) cirrus cloud base, (b) top, (c) geometrical thickness, and (d) optical depth, for the overall period (black), wet season (JFMA, red) and dry season (JJAS, blue).

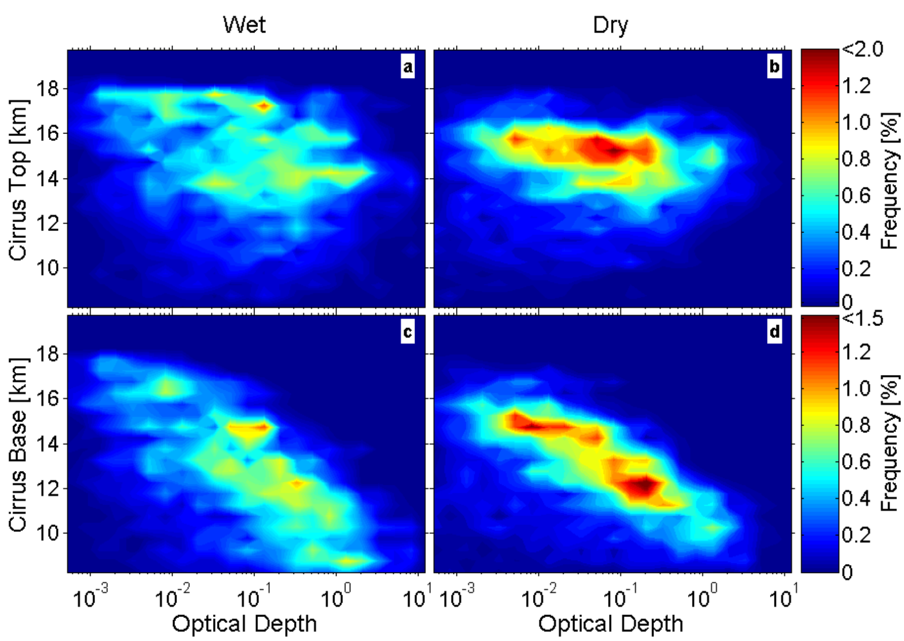

Figure 6. Two-dimensional histograms of cirrus cloud top (top) and cloud base (bottom) with optical depth during the wet (left) and dry (right) months are shown.

Atmos. Chem. Phys. Discuss., doi:10.5194/acp-2016-458, 2016
Manuscript under review for journal Atmos. Chem. Phys.
Published: 22 June 2016

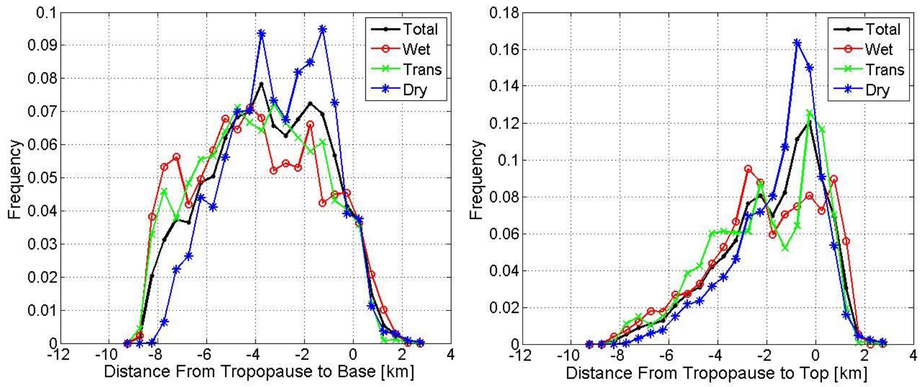

Figure 7. Normalized histograms of the distance of the tropopause to the cirrus base (left) and top (right) are shown for overall period (black) and each season (colors). Negative values mean that clouds are below tropopause. The average tropopause altitude was 16.2±0.4 km.

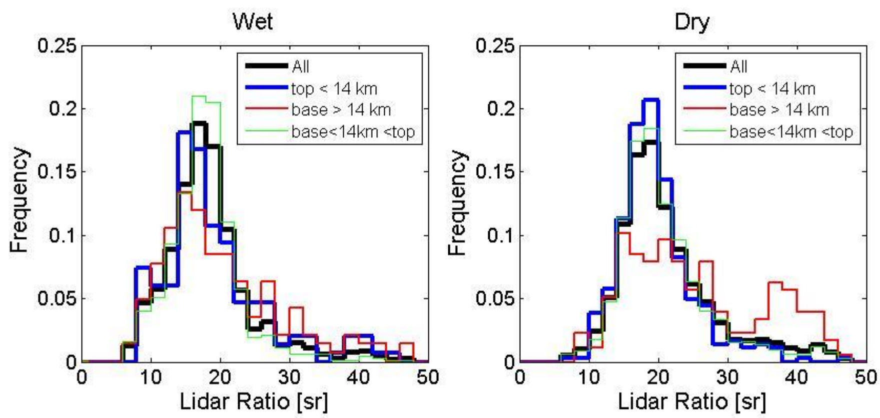

Figure 8. Normalized histograms of the lidar ratio for the wet (left) and dry (right) months are shown for all clouds (black) and clouds with base above 14 km (red), top below 14 km (blue) and cloud with top (base) above (below) 14 km (green).

Atmos. Chem. Phys. Discuss., doi:10.5194/acp-2016-458, 2016
Manuscript under review for journal Atmos. Chem. Phys.
Published: 22 June 2016

Atmospheric Chemistry and Physics
Open Access
Discussions

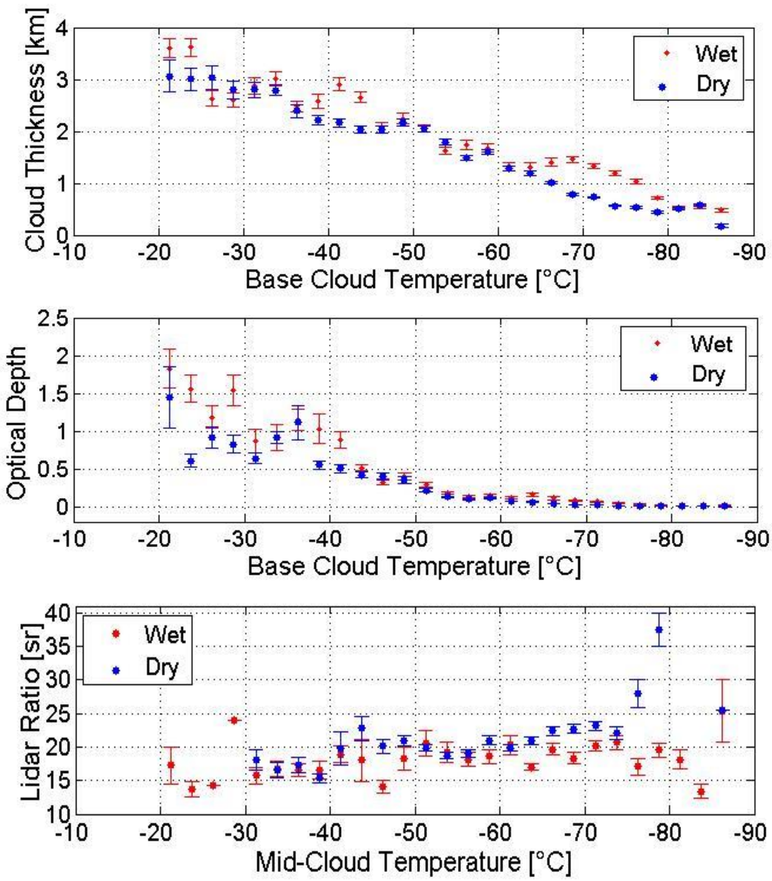

Figure 9. Dependence of the geometrical thickness, cloud optical depth and lidar ratio with temperature. Temperature are shown in 2.5 °C intervals and the other variables with their mean and standard deviation in each temperature interval.

1